Article

Not peer-reviewed version

Multivariate Evaluation of Pedogenetic Indicators: Limits and Potentials of Rare Earth Elements in Mountain Treeline Soils

Veneramaria Urso *, William Trenti, Mauro De Feudis, Gloria Falsone, Livia Vittori Antisari, Gianluca Bianchini

Posted Date: 5 March 2026

doi: 10.20944/preprints202603.0481.v1

Keywords: podzols; cambisols; coniferous forest; blueberry; sandstone

 doi:10.20944/preprints202603.0481.v1

Article

Multivariate Evaluation of Pedogenetic Indicators: Limits and Potentials of Rare Earth Elements in Mountain Treeline Soils

Veneramaria Urso [1,*], William Trenti [1], Mauro De Feudis [1], Gloria Falsone [1], Livia Vittori Antisari [1] and Gianluca Bianchini [2]

[1] Department of Agricultural and Food Sciences, Alma Mater Studiorum-University of Bologna, Viale Giuseppe Fanin 40, 40127 Bologna, Italy

[2] Department of Physics and Earth Science, University of Ferrara, Via Saragat 1, 44122 Ferrara, Italy

* Correspondence: veneramaria.urso2@unibo.it

Abstract

Vegetation strongly influences soil formation, yet its effect on Rare Earth Element (REE) distribution and fractionation across treeline ecotones remains insufficiently constrained. We investigated how contrasting plant communities, *Vaccinium myrtillus* heathlands and *Picea abies* forests, affect pedogenetic pathways and REE behavior in sandstone-derived soils of the Northern Apennines (Italy). Six soil profiles were characterized for bulk geochemistry, selective Fe–Al extractions, particle-size distribution, and REE concentrations. Principal component analysis and hierarchical clustering identified pedogenetic drivers and horizon groupings. Under *Vaccinium myrtillus*, thick acidic organic horizons promoted organo-metal complexation and incipient podzolization, whereas *Picea abies* soils showed thinner organic layers and enhanced mineral weathering, leading to Bw development with higher silt–clay contents and elevated Al/N ratios. These pathways were captured by Fe–Al indicators and the SpodicIndex. REE distributions showed vegetation-related differences in surface horizons and Eu–Ce anomalies but did not reproduce Fe–Al pedogenetic clusters, reflecting strong parent-material control. The coexistence of podzolic and cambic pathways at the treeline highlights pronounced spatial heterogeneity and vegetation effects. Plant composition may redirect pedogenesis, influencing nutrient cycling and metal mobility. Additionally, our findings emphasize the need to integrate multivariate statistics with established pedogenetic indicators when evaluating geochemical properties in mountain soils.

Keywords: podzols; cambisols; coniferous forest; blueberry; sandstone

1. Introduction

Rare Earth Elements (REEs) are increasingly used in pedogenetic studies because of their coherent geochemical behavior, relative immobility during primary weathering, and sensitivity to mineral transformations and organic matter dynamics [1]; [2]. Their vertical distribution along soil profiles can provide insights into the intensity and pathways of weathering, leaching, and secondary mineral formation, making them potentially informative tracers in mountain environments, where steep topography, vegetation variability and climatic gradients strongly influence soil development [3].

The abundance and fractionation of REEs in soils are primarily governed by parent material, mineralogical composition, grain size distribution and weathering intensity. In crystalline or highly weathered lithologies, REE patterns reflect the differential dissolution of accessory minerals, such as allanite, apatite and epidote for light REE (LREE), or xenotime for heavy REE (HREE), producing marked vertical variations during early alteration stages [2] .In contrast, soils formed on siliciclastic arenaceous formations, such as those of the Northern Apennines, inherit fewer REE-bearing minerals

 doi:10.20944/preprints202603.0481.v1

and undergo less differentiated weathering pathways; here, REE mobility is more strongly modulated by Fe–Al dynamics and organic–metal interactions.

Vegetation further modifies REE behavior by influencing soil acidity, organic matter inputs and the stability of organo-metal complexes [4]. Differences in litter quality, humification rates and surface-reactive organic compounds can alter REE complexation and redistribution, particularly in mountain environments where thick organic horizons often dominate the weathering process. Podzolization, as process driven by organic matter, may induce vertical decoupling between LREE and HREE due to their differing affinities for organic ligands and Fe/Al sesquioxides [3].

Despite this mechanistic background, the extent to which contrasting vegetation types influence REE fractionation and mobility across mountain treeline ecotones remains poorly constrained. In particular, the relative contribution of organic versus mineral carriers to REE redistribution under different pedogenetic pathways is not yet fully resolved [5].

Multivariate statistical approaches are increasingly adopted in soil science to interpret complex datasets, reduce dimensionality, and identify dominant gradients associated with soil-forming processes [6]. Ordination and clustering techniques such as principal component analysis (PCA) and hierarchical cluster analysis (CA) provide effective tools to discriminate pedogenetic pathways and to test the diagnostic value of geochemical indicators [7]. Within this framework, REE distributions can be critically evaluated by comparing REE-based patterns with pedogenetic groupings derived from independent mineralogical and geochemical variables.

The present study investigated how vegetation controls the distribution of REEs in mountain soils across the treeline ecotone of the Northern Apennines by comparing two contrasting plant communities: *Vaccinium myrtillus* heathlands and *Picea abies* forests. By integrating bulk geochemistry, selective Fe–Al extractions and multivariate statistical analyses (PCA and CA), we aim to (i) identify pedogenetic groupings based on established soil indicators, and (ii) assess whether REE-based patterns reproduce the same multivariate structure. This approach enables us to disentangle the controls governing REE mobility, fractionation patterns and elemental anomalies, and to evaluate the extent to which vegetation-driven differences in soil chemistry and weathering processes are reflected by REEs in high-elevation ecosystems.

2. Materials and Methods

2.1. Study Area and Site Localization

The study was conducted in the Northern Apennines (Italy), around Mount Cimone, the highest peak of the range (2165 m a.s.l.) (**Figure**). In this area the *Vaccinium myrtillus* (VM) heathlands and *Picea abies* (PA) spruce forests were selected. The PA stands represent relatively young, human-established forest covers, whereas the VM heathlands developed naturally and have persisted long enough to shape stable soil–vegetation feedbacks [8].

Six soil profiles were selected along an altitudinal gradient ranging from 1654 to 1939 m a.s.l. encompassing the transition from coniferous forest to high-altitude heathland. The treeline occurs around 1700 m a.s.l., marking the ecological boundary between forested and open subalpine habitats. Above the treeline, the landscape is characterized by VM-dominated heathlands, which play an important ecological and socio-economic role. VM is a widespread dwarf shrub commonly harvested by local communities for both fresh consumption and processing.

 doi:10.20944/preprints202603.0481.v1

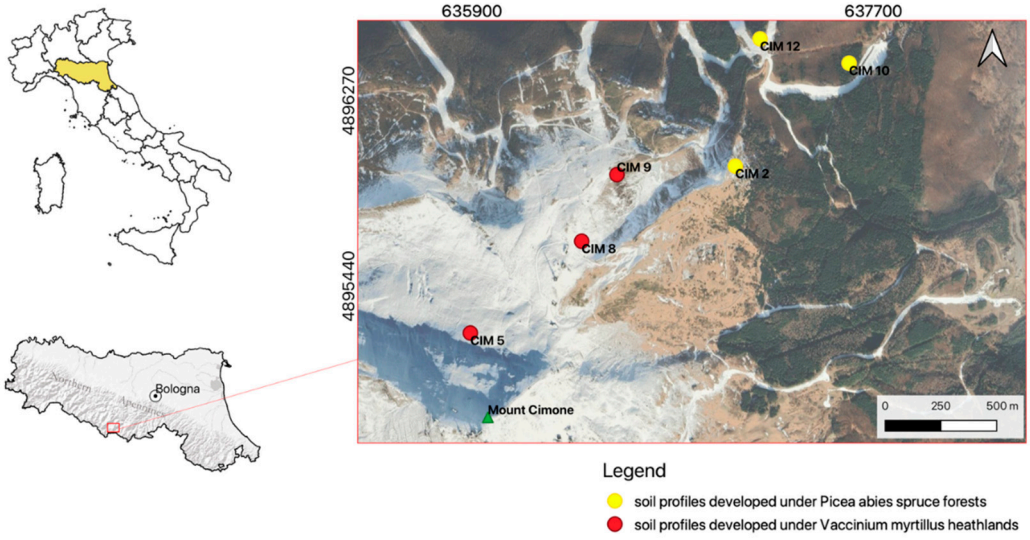

Figure 1. Geographic location of the six soil profiles investigated in the Northern Apennines.

The location and main characteristics of the six soil profiles are reported in Table 1. The sites differ in topographic position and slope steepness, thus representing a range of geomorphological and pedogenetic settings. All investigated soil profiles developed on sandstones Modino (MOD) formation, which is characterized by siliciclastic turbiditic sequences with variable sedimentary facies. Small local variations in facies and composition of MOD unit (e.g., arenaceous-dominant, marly interbedded, or glacially reworked facies), characterized the area, but parent material across the study area remains comparable from lithological view point.

Table 1. Geographic coordinates, elevation, vegetation cover, lithology, and topographic setting of the six soil profiles investigated in the Northern Apennines. VM = *Vaccinium myrtillus* heathland; PA = *Picea abies* spruce forest; MOD = Modino Unit. Slope position and steepness were determined in the field.

Profile	Coordinates		Altitude	Vegetation	Lithology	Slope position	Steepness
	m E	m N	m a.s.l.				°
CIM05	635892	4895230	1839	VM	MOD	Backslope	10
CIM08	636391	4895641	1846	VM	MOD	Backslope	10
CIM09	636549	4895939	1802	VM	MOD	Shoulder	5
CIM10	637590	4896438	1704	PA	MOD	Footslope	1
CIM02	637080	4895977	1679	PA	MOD	Shoulder	20
CIM12	637191	4896547	1654	PA	MOD	Shoulder	3

The morphological and physicochemical properties of the soil profiles are presented in Table 1S and 2S (Supplementary Materials). According to Soil Taxonomy (Soil Survey Staff, 2022), CIM2 and CIM12 were classified as Humic Lithic Dystrudepts, CIM10 as a Lithic Dystrudept, and CIM5, CIM8 and CIM9 as Lithic Humudepts. Despite similar parent material, vegetation and topographic setting exerted a clear influence on the development and weathering intensity of mineral horizons.

2.2. Soils Sampling and Analyses

The soils profiles were opened, described and sampled according to the recognition of different horizons, in 2015. Each soil's horizons were sampled and in lab analysed.

Table 1S reports international description of investigated soil profiles according to "Field book for describing and sampling soils" [9].

 doi:10.20944/preprints202603.0481.v1

2.3. Laboratory Analyses

All soil horizons were air-dried, gently disaggregated, and sieved to <2 mm prior to chemical and isotopic analyses. For organic horizons, samples were finely ground in an agate mill.

Total organic carbon (TOC) and total nitrogen (TN) contents were determined using an elemental analyzer (Flash EA 1112 Series, Thermo Fisher Scientific, USA).

Soil pH was measured potentiometrically in a 1:2.5 soil-to-water suspension (w/v) using a combined glass electrode. Particle-size distribution was determined by the pipette method after dispersion with sodium hexametaphosphate [10]. The cation exchange capacity (CEC) and exchangeable base cations (Ca^{2+}, Mg^{2+}, K^{+}, and Na^{+}) were determined by extraction with 1 M NH_4OAc at pH 7.0 [11].. Exchangeable cations were quantified by inductively coupled plasma optical emission spectrometry (ICP-OES; Arcos, Spectro Analytical Instruments). Base saturation (GBS, %) was calculated as the sum of exchangeable base cations divided by CEC × 100.

Pedogenic and poorly crystalline forms of Fe and Al were determined by selective extractions: dithionite–citrate–bicarbonate extraction (Fed, Ald; [12]) to quantify total pedogenic oxides, and acid ammonium oxalate extraction in darkness (Feo, Alo; [13]) to target amorphous and organo-complexed forms, and Na-pyrophosphate (Alp and Fep), per [14]. Extracts were analyzed by ICP-OES (Arcos, Spectro Analytical Instruments). The ratio Feo/Fed was used as an indicator of the degree of weathering and oxide crystallinity.

For mineral horizons, pseudo-total concentrations of major and trace elements were obtained after aqua regia digestion ($HCl:HNO_3$ = 3:1, v/v) at 95 °C, following ISO 11466 (1995). For organic horizons, samples were digested using a mixture of concentrated HNO_3 and H_2O_2 (3:1, v/v) at 120 °C to ensure complete oxidation of organic matter (USEPA 3050B). The resulting solutions were analyzed by ICP-OES (Arcos, Spectro Analytical Instruments) for major elements (Al, Fe, Ca, Mg, K, Na, P, S). Certified reference materials [15] were used for quality control, with recovery rates between 90% and 110%.

2.4. Rare Earth Elements Analysis

Sample preparation for REE analysis (La, Ce, Pr, Nd, Sm, Eu, Gd, Tb, Dy, Ho, Er, Tm, Yb and Lu) was carried out in a clean laboratory. Approximately 250 mg of finely ground sample powder (<2 mm fraction, homogenized using an agate mortar and pestle) was first treated with 30% H_2O_2 to remove organic matter, and then digested in a mixture of concentrated HCL and HNO. The resulting solutions were analyzed for REE concentrations using inductively coupled plasma–mass spectrometry (ICP-MS iCAP TQ (Thermo Fisher Scientific).

Accuracy and precision, based on repeated analyses of certified reference materials and standards, were better than 10% for all considered elements. Procedural blanks contained negligible REE concentrations relative to the samples.

REE concentrations were normalized both to an external reference (Upper Continental Crust, UCC; [16]; [17]) and to the local parent material, following [18], [19], and [20]. Normalized concentrations were plotted in distribution patterns with REE ordered by increasing atomic number.

2.5. Data Processing

The Spodic Index (SI) was calculated to assess the degree of spodic horizon development. Following Soil Taxonomy [21] SI was defined as the sum of oxalate-extractable aluminum (Alo) and half of oxalate-extractable iron (½Feo).

REEs were grouped into LREEs (La, Ce, Pr, Nd, Sm and Eu) and HREE (Gd, Tb, Dy, Ho, Er, Tm, Yb and Lu). Fractionation between REE groups was evaluated using LREE/HREE ratios and the total REE concentration (ΣREE). Elemental ratios (La/Gd) and anomalies for europium (Eu/Eu*) (1) and cerium (Ce/Ce*) (2) were calculated following [22], [23] and [24].

Europium anomalies (Eu/Eu*) were computed after normalization as:

 doi:10.20944/preprints202603.0481.v1

$$Eu/Eu^* = \frac{Eu_N}{\sqrt{Sm_N \times Gd_N}} \quad (1)$$

Cerium anomalies (Ce/Ce*) were calculated as:

$$Ce/Ce^* = \frac{Ce_N}{(La_N + Pr_N)/2} \quad (2)$$

where the subscript N denotes normalized concentrations. Positive anomalies, values >1, indicate relative Eu or Ce enrichment, whereas values < 1 indicate Eu or Ce depletion [25]; [26].

2.6. Statistical Analyses

We combined ordination (PCA and CA), and non-parametric tests to derive data-driven horizon groupings and to formally assess whether REE-based patterns reproduce the same pedogenetic structure identified by established soil indicators [6].

All statistical analyses were performed in RStudio (version 2025.09.0+387; released 12 September 2025). PCA and CA were first applied to all soil horizons using physicochemical properties and nutrient-related variables (organic C, total N, P, Ca, Fe, Al, and C/N, C/P and Al/N ratios; Table 3S). A second multivariate analysis was then conducted exclusively on organo-mineral (A), mineral (B) and pedogenetic substrate (C) horizons, using selected physicochemical variables (pH, GSB, exchangeable Ca, sand and clay fractions, organic C and total N) together with pedogenic Fe–Al fractions (Alo/Feo, Alp/Fep, Ald/Fed) and the Spodic Index (Table 4S).

Clusters were defined through hierarchical clustering based on Euclidean distances calculated on standardized variables and were subsequently validated by PCA ordination. Differences among clusters were tested using the non-parametric Kruskal–Wallis test, applied to identify statistically significant contrasts among groups.

3. Results

3.1. Distribution Patterns of Biogenic Nutrients and Weathering-Related Elements

Both VM and PA soils developed thick Oi horizons, although with slightly different mean thicknesses and a high variability (2.9 ± 2.2 cm and 2.0 ± 1.3 cm, respectively). In both vegetation types, the Oe layer was the thickest organic horizon, with greater thickness under VA (5.3 ± 2.3 cm) than under PA (2.6 ± 2.1 cm). All profiles contained the three typical organic horizons (Oi, Oe, Oa), except profile CIM10, in which only an Oe horizon could be separated due to indistinct boundaries.

Below organic horizons, in all soil profiles A or transitional AE or AB horizons were present, overlying Bs or Bw horizons depending on vegetation cover (Bhs or Bs in VM and Bw in PA; Table 1S). C horizons were at the bottom of soil profiles.

The distribution patterns of biogenic nutrients (C, N, P, S) and weathering-related elements (Al, Fe) varied primarily along soil horizons (Table 3S).

Vegetation effects were evaluated by applying the Kruskal–Wallis test to compare elements distribution under VM and PA within corresponding horizon types. Most nutrient variables did not differ significantly between vegetation types. Significant differences were detected only for total N and P in Oi horizons (N: 0.8 vs. 1.6%; P: 0.5 vs. 0.9 g kg^{-1}, respectively for VM and PA) and for total Fe in A and eluvial horizons (16.7 and 18.3 vs 23.3 g kg^{-1}, respectively for VM and PA; Figure 1S).

To further explore the joint variation among physicochemical parameters and to identify potential horizon groupings independent of vegetation type, CA and PCA were performed on the full dataset (Figure 2S and **Figure**). These multivariate approaches allowed the dominant gradients structuring soil variability to be identified and the relative influence of organic versus mineral components to be assessed.

 doi:10.20944/preprints202603.0481.v1

The axis 1 of PCA (Dim1, 67.5 % of the total variance) described a dominant organic-to-mineral gradient, characterized by decreasing C, N and P contents and increasing Al and Fe concentrations. The axis 2 (Dim2, 18.2%) captured more subtle variations associated with nutrient stoichiometry (P and S) and the Al/N ratio.

The resulting clusters reflected this geochemical structure (**Figure**). Cluster A comprised litter horizons (Oi), which separated clearly along Dim1 due to their very high C, N and P contents and elevated C/N and C/P ratios. Cluster B grouped partially decomposed and humified organic horizons (Oe and Oa), characterized by elevated N and S and intermediate C/N and C/P ratios. Cluster C included organo-mineral horizons and illuvial B horizons of VM soils, representing the transition from organic-dominated layers to horizons with increasing Al and Fe accumulation. Cluster D comprised mineral subsoil horizons, characterized by the highest Al, Fe and Al/N values and the lowest concentrations of biogenic elements.

Cluster composition varied with vegetation type. Soil horizons under VM mostly belonged to cluster C, including their B horizons, whereas the deepest mineral horizons of profiles CIM10 and CIM12 grouped within cluster D. Their overlying organo-mineral horizons clustered instead within cluster C, indicating intermediate chemical characteristics. Profile CIM2 (under PA) also clustered with more organic-rich horizons, reflecting shallow soil development and a strong influence of surface organic inputs.

Overall, these results highlight a well-defined vertical sequence from organic-rich horizons to mineral horizons dominated by pedogenic Al and Fe, with vegetation modulating horizon thickness, chemical composition and vertical arrangement along this gradient.

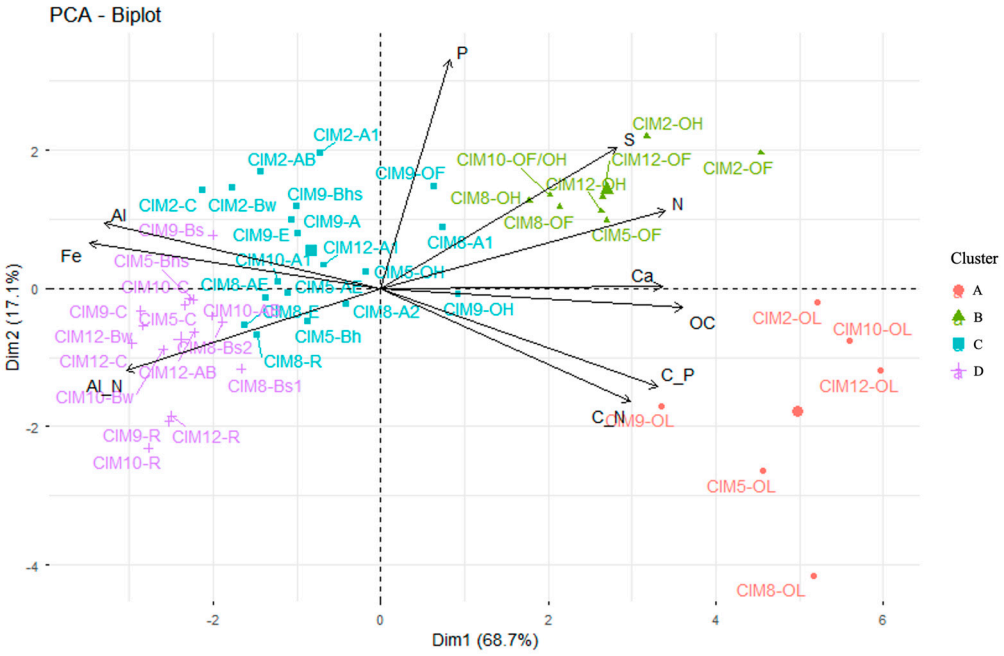

Figure 2. Principal component analysis carried out on the concentration of organic C (OC), N, P, S, Ca, Al and Fe, and on Al/N (Al_N), C/N (C_N), C/P (C_P) ratios across all soil horizons formed under VM (*Vaccinium myrtillus*) and PA (*Picea abies*). Scores are displayed along Dim1 (68.7% of variance) and Dim2 (17.1%). Arrows represent variable loadings. OL, OF, OH correspond to Oi, Oe, Oa horizons respectively.

To quantify the geochemical differences identified by the multivariate analysis (**Figure**), the main chemical properties of the four clusters were compared using non-parametric statistics (**Table**). Cluster A showed the highest organic C contents and the highest C/N and C/P ratios, together with the lowest Al, Fe and Al/N values. Clusters A and B, than clusters grouping Oi, Oe and Oa horizons, exhibited significantly higher N, Ca, P and S concentrations than the clusters, C and D, grouping

 doi:10.20944/preprints202603.0481.v1

mineral horizons. However, cluster B showed intermediate Al and Fe contents and Al/N ratios. It confirmed the higher degradation of organic matter in Oe and Oa horizons (cluster B) than in Oi (cluster A) and the higher interaction with the mineral phase.

Clusters C and D differed more markedly. Although they showed similar Ca and Fe concentrations, cluster D was characterized by significantly lower C, N, P and S contents and higher Al and Al/N values, consistent with a stronger mineral control and reduced organic influence on horizon properties.

The differences among clusters indicate a progressive shift in element distribution from nutrient-rich organic horizons to deeper mineral horizons increasingly shaped by pedogenic processes related to Al–Fe.

Table 2. Mean values of organic C (OC), N, P, S, Ca, Al and Fe contents, and of Al/N, C/N, C/P ratios for the four clusters identified in the multivariate analysis (Figure 2). Different letters within each column indicate significant differences among clusters ($p < 0.05$).

Cluster	OC (%)	N (%)	P (g/kg)	S (g/kg)	Ca (g/kg)
A	47.7 a	1.2 a	0.71 bc	0.80b	7.7 a
B	25.1 b	1.3 a	1.0 a	1.24 a	5.3 a
C	6.0 c	0.4 b	0.93 ab	0.48 c	1.1 b
D	4.2 d	0.2 c	0.71 c	0.35 d	0.9 b
Cluster	Al (g/kg)	Fe (g/kg)	Al/N	C/N	C/P
A	3.6 d	2.3 c	0.32 d	41.1 a	662a
B	24.4 c	12.2 b	2.05 c	19.2 b	255b
C	38.9 b	21.3 a	9.8 b	13.9 c	69c
D	44.8 a	23.9 a	21.7 a	15.4 c	56c

3.2. Weathering Indicators and Horizon Differentiation

To further resolve pedogenetic differentiation in the mineral part of the profiles, PCA and CA exclusively to organo-mineral and mineral horizons were applied (**Figure**).

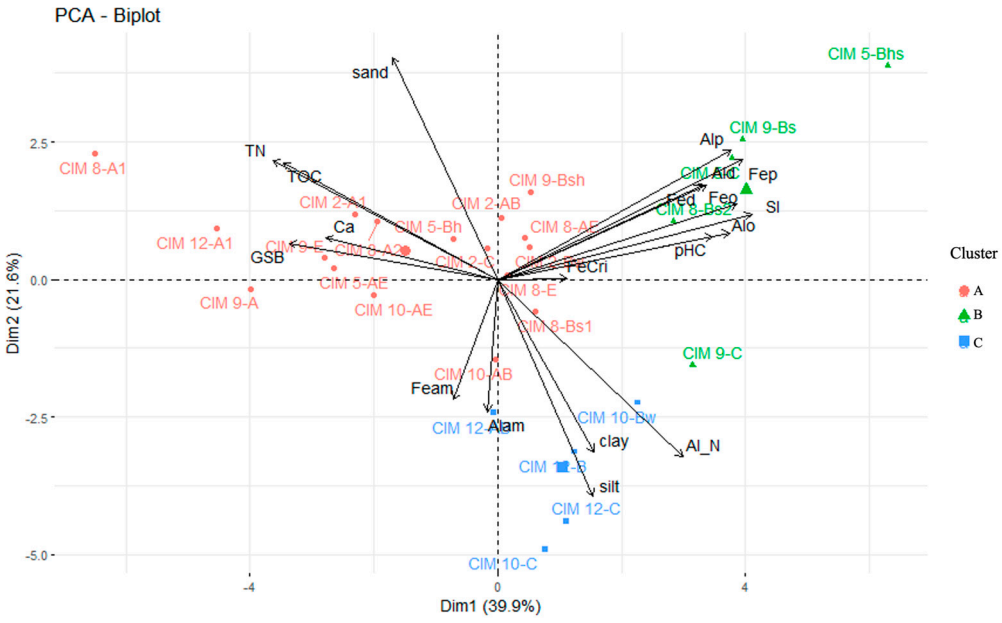

Figure 3. Cluster analysis and principal component analysis of physicochemical properties of organo-mineral and mineral soil horizons. TN = total N; TOC = total organic; GSB = base saturation; Alo and Feo= oxalate-extractable Al and Fe, respectively: Alp and Fep = Na-pyrophosphate-extractable Al and Fe, respectively; Alam and Feam = amorphous iron and aluminum (Alo-Alp, and Feo-Fep); Ald and Fed = dithionite–citrate–bicarbonate-extractable Al and Fe, respectively; FeCri = well crystalline Fe oxides (Fed-Feo) iron; SI = spodic index.

 doi:10.20944/preprints202603.0481.v1

Three clusters were identified. Cluster A comprised surface mineral horizons (A, E, AB) across both vegetation types and was characterized by higher sand content, greater total organic C and N, higher exchangeable Ca, and higher base saturation. Cluster B included the subsoil horizons of CIM5, CIM8 and CIM9 (VM), which were strongly associated with pedogenic Fe–Al phases and high Spodic Index values. Cluster C grouped the subsoil horizons of CIM10 and CIM12 (PA), which showed elevated silt and clay, and in general the higher content of pedogenic Al and Fe oxides indicating more intense *in situ* weathering and Bw development.

The variables that significantly differentiated the three mineral clusters are reported in **Table** . Subsoil horizons under VM (cluster B) displayed higher Alo, Feo and SI values, whereas PA-dominated subsoil horizons (cluster C) showed significantly higher silt and clay. These patterns indicate the coexistence of two contrasting pedogenetic pathways: podzolisation conditions under VM heathlands and mineral-weathering-dominated conditions under PA forests.

Table 3. Kruskal–Wallis test for chemical, mineralogical, and physical properties significantly differentiating the three soil clusters (Figure). Different letters within each column indicate significant differences among clusters ($p < 0.05$). The Table reports selective extractions of aluminum and iron (Alo and Feo= oxalate-extractable Al and Fe, respectively; Alp and Fep = Na-pyrophosphate-extractable Al and Fe, respectively; Ald and Fed = dithionite–citrate–bicarbonate-extractable Al and Fe, respectively), particle-size distribution (clay and sand), the Spodic Index (Alo+1/2Feo), and basic soil chemical parameters (pH, OC = organic carbon, N = total nitrogen).

Cluster	Alo (g/kg)	Alp (g/kg)	Ald (g/kg)
A	4.4 b	8.4 b	3.7 b
B	7.5 a	14.7 a	6.7 a
C	5.1 b	9.7 b	3.5 b
	Feo (g/kg)	Fep (g/kg)	Fed (g/kg)
A	7.9 b	5.9 b	8.9 b
B	14.3 a	12.5 a	15.1 a
C	9.2 b	6.2 b	10.7 b
	Clay (g/kg)	Sand (g/kg)	Spodic Index
A	46 b	737 a	8.4 b
B	46 b	746 a	14.7 a
C	111 a	517 b	9.7 b
Cluster	pH	OC	N
A	4.4 b	6.0 a	0.4 a
B	4.7 ab	4.3 ab	0.3 ab
C	4.8 a	2.9 b	0.2 b

3.3. Rare Earth Element Dynamics Along Soil Profiles

To assess how REEs respond to the pedogenetic contrasts identified in Sections 3.1 and 3.2, the vertical distributions of LREE, HREE, ΣREE, the La:Yb ratio, and redox-sensitive anomalies (Eu*, Ce*) were examined along individual profiles (Figure 3S). Differences between soil horizons under vegetation types were evaluated using the Kruskal–Wallis test.

LREE and HREE concentrations were generally higher under VM than under PA, particularly in A–E and C horizons (e.g., LREE: 0.67 ± 0.09 *vs*. 0.61 ± 0.07 mg kg^{-1} in upper mineral layers; 0.75 ± 0.02 *vs*. 0.65 ± 0.04 mg kg^{-1} in C horizons). Total REE concentrations (ΣREE) were significantly higher in C horizons under VM (6.37 ± 0.7 mg kg^{-1}) compared with PA (5.37 ± 0.4 mg kg^{-1}). In organic horizons, Oe and Oa layers showed higher REE contents than Oi horizons.

 doi:10.20944/preprints202603.0481.v1

Eu anomalies (Eu*) were positive in Oa horizons under PA (1.07) but negative under VM (0.83). Ce anomalies (Ce*) were always negative and showed marked higher values in B and C horizons under PA. In VM soil profiles, Ce* displayed a slight increase in C horizons relative to the other mineral horizons (0.26 *vs*. 0.23). Beyond these differences, no additional significant contrasts between vegetation types were detected.

When REE variables were examined across the four clusters derived from the first multivariate analysis (**Figure**), Oi horizons (cluster A) were characterized by very low REE concentrations and positive Eu anomalies. REE contents increased in organo-mineral and mineral clusters (C and D), indicating a general enrichment with depth. However, Kruskal–Wallis tests applied to the three mineral clusters identified in Section 3.2, and thus excluding organic horizons, revealed no significant differences for ΣREE or LREE/HREE ratios (Table 5S). Only Ce* differed significantly among mineral clusters, being elevated in subsurface horizons under PA (**Figure**).

Overall, REE distributions exhibited consistent vertical gradients (**Figure**), but did not distinguish the pedogenetic groupings identified by Fe–Al indicators and the Spodic Index, suggesting that REE variability is primarily controlled by mineralogical and depth-related factors rather than by horizon differentiation processes.

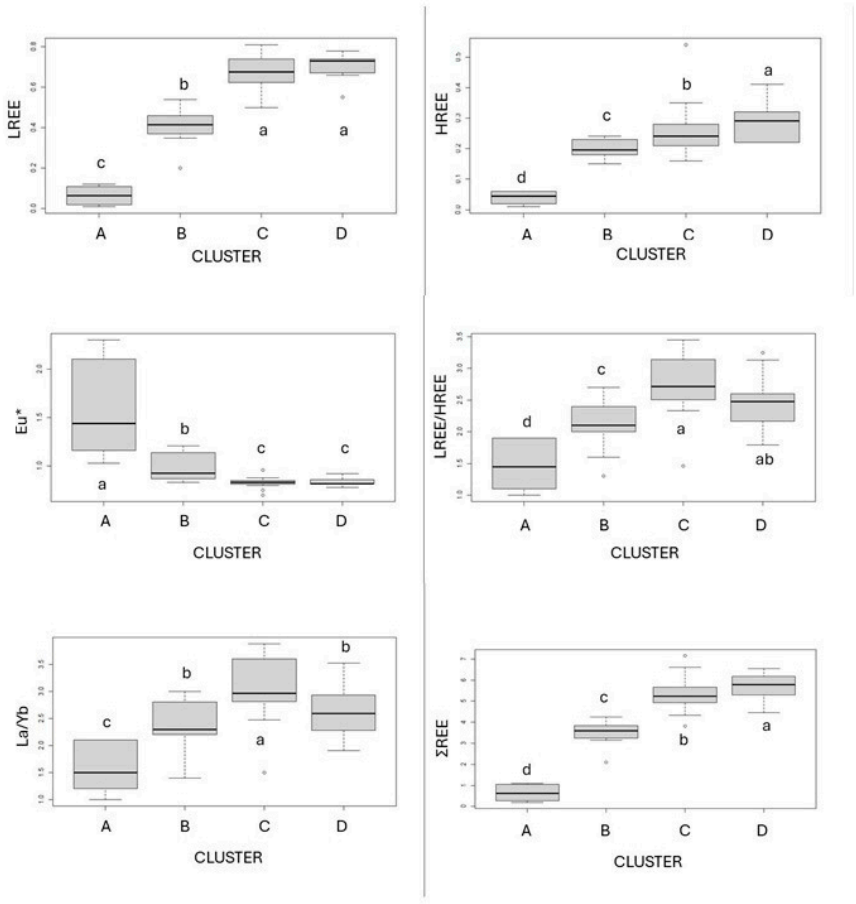

Figure 4. Vertical distribution of Rare Earth Elements (REE), expressed as mg kg-1, across the four clusters identified in Section 3.1 by multivariate analyses, where cluster A is litter, B is organic horizons, C is organ mineral horizons and D is mineral horizons and D is mineral horizons. Different lowercase letters indicate significant differences among clusters ($p < 0.05$). LREE = light REE; HREE = heavy REE.

 doi:10.20944/preprints202603.0481.v1

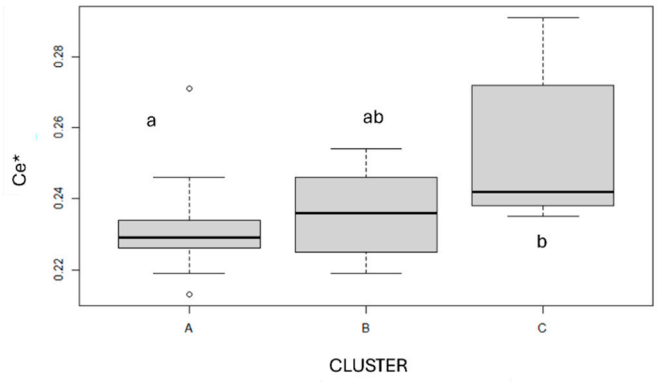

Figure 5. Distribution of Cerium anomalies (Ce*) across the three clusters identified in Section 3.2 by multivariate analyses, where cluster A is organo-mineral horizons, B is spodic horizons under VM, C is mineral horizons mainly under PA. Different lowercase letters indicate significant differences among clusters ($p < 0.05$).

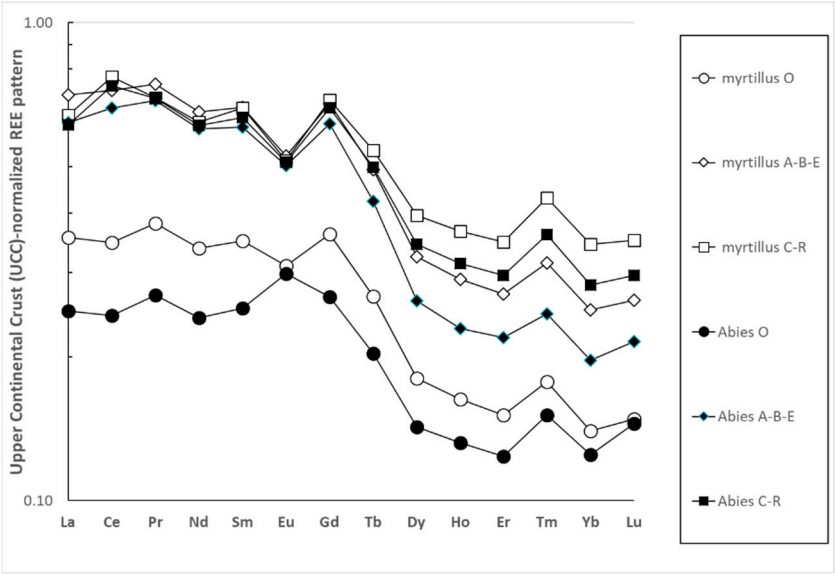

Figure 6. Upper Continental Crust (UCC)-normalized Rare Earth Element (REE) patterns for soils developed under *Vaccinium myrtillus* and *Picea abies*, grouped by major pedological horizons (O, A–B–E, C–R).

4. Discussion

4.1. Vegetation Controls on Surface Soils Development and Nutrient Stoichiometry

Vegetation exerted a control on the development and chemical signature of organic horizons. Soils under *Vaccinium myrtillus* exhibited thicker O horizons, especially Oe—than those under *Picea abies*, reflecting species-specific differences in litter input and decomposition dynamics [27]. Oi horizons under *Vaccinium myrtillus* were characterized by lower total N and P contents compared with *Picea abies*, reflecting limited nutrient availability in the litter.

These patterns agree with [28], who showed that tree and shrub species strongly influence humus form differentiation in Italian forests through effects on litter quality, soil acidity and faunal activity. The thick, poorly incorporated organic materials under VM align with Moder-like conditions characterized by reduced faunal mixing and stratified organic horizons [29]. In contrast, the thinner organic horizons and P total content observed under PA would suggest more efficient litter incorporation in mineral soil and a tendency toward Amphimull-like forms. Overall, vegetation-

 doi:10.20944/preprints202603.0481.v1

driven differences in litter quantity and biochemical composition play a central role in the differentiation of surface horizons at the treeline.

4.2. Transition from Organic to Mineral Horizons: Contrasting Pathways of Al–Fe Accumulation

The transition from organic to mineral horizons revealed two distinct pedogenetic trend associated to vegetation type. Under VM, elevated Alo and Feo contents together with higher Spodic Index values indicate the formation of organo-metal complexes and the onset of podzolization. In these soils, Al and Fe are mobilized from upper horizons and retained as organo-metal associations in subsurface layers, consistent with cheluviation–chilluviation process [3].

In contrast, subsurface horizons under PA were characterized by higher silt and clay contents, elevated Al/N ratios and the absence of diagnostic spodic features. These characteristics are consistent with enhanced *in situ* mineral weathering and the development of Bw horizons, rather than with the downward translocation of Al–Fe–organic complexes. Thus, vegetation appears to influence not only the intensity but also the mechanism of Al–Fe accumulation in subsurface horizons, promoting podzolic differentiation under *Vaccinium* and mineral alteration under *Picea*.

4.3. Al/N Ratio as an Indicator of Aluminum Mobility and Early Horizon Differentiation

The Al/N ratio provided an additional indicator to distinguish the pedogenetic pathways under VM and PA. Elevated Al/N values in subsurface horizons under PA corresponded to clay- and silt-enriched Bw horizons identified in the multivariate analysis, reflecting enhanced *in situ* mineral weathering and increased pools of reactive Al [30].

By contrast, VM soils exhibited moderate Al/N values in A and E horizons, where Al remains predominantly associated to organo-metal complexes, as indicated by higher Alo, Feo and Spodic Index values. The comparatively limited increase of Al/N with depth under VM reflects the dominance of organic–metal translocation processes. When interpreted together with Fe–Al selective extractions and SI, the Al/N ratio effectively differentiates Al enrichment driven by organic complexation from that resulting from *in situ* weathering.

4.4. Limited Ability of Rare Earth Elements to Track Pedogenetic Differentiation

In light of the contrasting pedogenetic pathways identified under the two vegetation types, the ability of REEs to trace horizon differentiation was critically assessed. Although some vegetation-related contrasts were observed (i.e., soil profiles in VM displayed higher LREE and HREE in the A and E horizons and higher ΣREE in the C horizons), these patterns primarily reflect differences in surface organic inputs and litter chemistry rather than subsurface processes. This is consistent with findings that REE signatures in upper soil layers respond to litter quality and degradation pathways [31]; [2].

Across all profiles, Eu anomalies decreased with depth, indicating progressive feldspar weathering, while Ce anomalies varied markedly under PA and increased slightly in the C horizons under VM. However, multivariate analyses revealed no significant differences among clusters for ΣREE, LREE/HREE, Eu* or La/Yb, and only Ce* distinguished the subsurface spruce horizons. Importantly, these REE trends did not reproduce the pedogenetic groupings identified by the other physico-chemical properties: horizons clustering based on Al, Fe, SI and texture showed no corresponding separation in ΣREE, LREE/HREE or anomaly patterns, confirming that REEs respond to different controls than those driving horizon differentiation. The absence of coherent REE gradients along pedogenic boundaries confirms that REEs reflect broad mineralogical or depth-related controls rather than the specific processes that differentiate podzolic and cambic horizons. By contrast, Fe–Al selective extractions and SI captured clear and consistent pedogenetic signatures.

 doi:10.20944/preprints202603.0481.v1

4.5. Implications for Pedogenesis at the Treeline in the Northern Apennines

The results highlight the pivotal role of vegetation in driving pedogenesis at the treeline. VM promotes thicker acidic organic horizons and facilitates the formation of organo-metal complexes, leading to incipient podzolization. In contrast, PA favors mineral weathering and Bw development due to thinner organic layers and greater exposure of mineral surfaces. PA stands, being relatively recent reforestation systems, have not yet developed the organic–mineral translocation conditions required for podzolization. These vegetation-driven differences explain why Fe–Al indicators effectively track horizon differentiation, whereas REEs primarily reflect depth-related and mineralogical controls.

The coexistence of podzolic and cambic pathways within a short altitudinal span illustrates the strong spatial heterogeneity of soils at the treeline and underscores how vegetation composition governs the balance between organic–metal translocation and mineral alteration. In this sandstone-dominated landscape, Fe–Al pedogenic phases, rather than REEs, emerge as the most reliable proxies for weathering intensity and soil evolution.

5. Conclusions

This study demonstrates that vegetation exerts a primary control on early soil development at the treeline of the Northern Apennines. VM promotes thick acidic organic horizons and organo-metal complex formation, leading to incipient podzolization, whereas PA favors mineral weathering and Bw development under thinner organic layers. These contrasting pathways occur over short spatial scales, highlighting how vegetation-mediated biogeochemical processes can diverge Al–Fe distributions and pedogenetic trajectories even under the same parent material and climate.

REE patterns show clear vertical trends, with depletion in surface O horizons and enrichment in deep C horizons, reflecting strong parent-material control. Although vegetation influences REE concentrations in upper horizons, REE distributions do not reproduce the pedogenetic groupings identified by Fe–Al selective extractions and the Spodic Index. Only Ce* showed partial sensitivity to subsurface variability. Overall, REEs appear to be weak tracers of pedogenetic differentiation in these sandstone-derived mountain soils, whereas Fe–Al phases provided more reliable indicators of horizon development and weathering intensity.

The coexistence of podzolic and cambic pathways at the treeline highlights the strong spatial heterogeneity of mountain soils and underscores the role of vegetation history in shaping soil evolution. Differences between long-established heathlands and relatively recent spruce reforestation stands further suggest that shifts vegetation legacies, and that shifts in vegetation composition can redirect pedogenetic processes, potentially altering nutrient cycling, metal mobility and associated ecosystem functions. Further research integrating soil solution chemistry, microbial dynamics and long-term vegetation monitoring will help clarify how these coupled vegetation-soil systems respond to future environmental change in high-elevation landscapes.

Supplementary Materials: The following supporting information can be downloaded at the website of this paper posted on Preprints.org.

References

1. Aubert, D.; Stille, P.; Probst, A.; Gauthier-lafaye, F.; Pourcelot, L.; Del Nero, M. Characterization and Migration of Atmospheric REE in Soils and Surface Waters. *Geochim. Cosmochim. Acta* **2002**, *66*, 3339–3350, doi:10.1016/S0016-7037(02)00913-4.
2. Tyler, G. Rare Earth Elements in Soil and Plant Systems-A Review. *Plant Soil* **2004**, *267*, 191–206.
3. Aide, M.T.; Aide, C. Rare Earth Elements: Their Importance in Understanding Soil Genesis. *ISRN Soil Sci.* **2012**, *2012*, 1–11, doi:10.5402/2012/783876.
4. Kabata-Pendias, A. *Trace Elements in Soils and Plants*; CRC press, 2000;

 doi:10.20944/preprints202603.0481.v1

5. Sager, M.; Wiche, O. Rare Earth Elements (REE): Origins, Dispersion, and Environmental Implications—A Comprehensive Review. *Environments* **2024**, *11*, 24.
6. Milinovic, J.; Vale, C.; Azenha, M. Recent Advances in Multivariate Analysis Coupled with Chemical Analysis for Soil Surveys: A Review. *J. Soils Sediments* **2023**, *23*, 1085–1098, doi:10.1007/s11368-022-03377-8.
7. Souza, T. *Advanced Statistical Analysis for Soil Scientists*; Springer Nature Switzerland: Cham, 2025; ISBN 978-3-031-88160-2.
8. Antisari, L.V.; Agnelli, A.; Corti, G.; Falsone, G.; Ferronato, C.; Marinari, S.; Vianello, G. Modern and Ancient Pedogenesis as Revealed by Holocene Fire - Northern Apennines, Italy. *Quat. Int.* **2018**, *467*, 264–276, doi:10.1016/j.quaint.2017.12.050.
9. Schoeneberger, P.J.; Wysocki, D.A.; Benham, E.C. *Field Book for Describing and Sampling Soils*; Government Printing Office, 2012;
10. Gee, G.W.; Bauder, J.W. Particle-Size Analysis. *Methods Soil Anal. Part 1 Phys. Mineral. Methods* **1986**, *5*, 383–411.
11. Sumner, M.E.; Miller, W.P. Cation Exchange Capacity and Exchange Coefficients. *Methods Soil Anal. Part 3 Chem. Methods* **1996**, *5*, 1201–1229.
12. Mehra, O.; Jackson, M. Iron Oxide Removal from Soils and Clays by a Dithionite–Citrate System Buffered with Sodium Bicarbonate. In *Clays and clay minerals*; Elsevier, 2013; pp. 317–327.
13. Blakemore, L. Methods for Chemical Analysis of Soils. *NZ Soil Bur Sci Rep* **1981**, *10*.
14. Bascomb, C. Distribution of Pyrophosphate-Extractable Iron and Organic Carbon in Soils of Various Groups. *J. Soil Sci.* **1968**, *19*, 251–268.
15. Vittori Antisari, L.; Bianchini, G.; Dinelli, E.; Falsone, G.; Gardini, A.; Simoni, A.; Tassinari, R.; Vianello, G. CRITICAL EVALUATION OF AN INTERCALIBRATION PROJECT FOCUSED ON THE DEFINITION OF NEW MULTI-ELEMENT SOIL REFERENCE MATERIALS (AMS-MO1 AND AMS-ML1). *EQA - Int. J. Environ. Qual.* **2014**, 41-64 Pages, doi:10.6092/ISSN.2281-4485/4553.
16. Rudnick, R.L.; Gao, S. Composition of the Continental Crust. In *Treatise on Geochemistry*; Elsevier, 2003; pp. 1–64 ISBN 978-0-08-043751-4.
17. Laveuf, C.; Cornu, S. A Review on the Potentiality of Rare Earth Elements to Trace Pedogenetic Processes. *Geoderma* **2009**, *154*, 1–12, doi:10.1016/j.geoderma.2009.10.002.
18. Braun, J.-J.; Viers, J.; Dupré, B.; Polve, M.; Ndam, J.; Muller, J.-P. Solid/Liquid REE Fractionation in the Lateritic System of Goyoum, East Cameroon: The Implication for the Present Dynamics of the Soil Covers of the Humid Tropical Regions. *Geochim. Cosmochim. Acta* **1998**, *62*, 273–299.
19. Aubert, D.; Stille, P.; Probst, A. REE Fractionation during Granite Weathering and Removal by Waters and Suspended Loads: Sr and Nd Isotopic Evidence. *Geochim. Cosmochim. Acta* **2001**, *65*, 387–406, doi:10.1016/S0016-7037(00)00546-9.
20. Dequincey, O.; Chabaux, F.; Leprun, J.-C.; Paquet, H.; Clauer, N.; Larqué, P. Lanthanide and Trace Element Mobilization in a Lateritic Toposequence: Inferences from the Kaya Laterite in Burkina Faso. *Eur. J. Soil Sci.* **2006**, *57*, 816–830.
21. Taxonomy, S. Keys to Soils Taxonomy . United States Deparment of Agriculture. *Nat. Resour. Conserv. Serv.* **2014**.
22. Mourier, B.; Poulenard, J.; Chauvel, C.; Faivre, P.; Carcaillet, C. Distinguishing Subalpine Soil Types Using Extractible Al and Fe Fractions and REE Geochemistry. *Geoderma* **2008**, *145*, 107–120, doi:10.1016/j.geoderma.2008.03.001.
23. Ndjigui, P.-D.; Bilong, P.; Bitom, D.; Dia, A. Mobilization and Redistribution of Major and Trace Elements in Two Weathering Profiles Developed on Serpentinites in the Lomié Ultramafic Complex, South-East Cameroon. *J. Afr. Earth Sci.* **2008**, *50*, 305–328.
24. Vázquez-Ortega, A.; Perdrial, J.; Harpold, A.; Zapata-Ríos, X.; Rasmussen, C.; McIntosh, J.; Schaap, M.; Pelletier, J.D.; Brooks, P.D.; Amistadi, M.K.; et al. Rare Earth Elements as Reactive Tracers of Biogeochemical Weathering in Forested Rhyolitic Terrain. *Chem. Geol.* **2015**, *391*, 19–32.
25. Zhao, Y.-Y.; Zheng, Y.-F. Geochemistry of Vein and Wallrock Carbonates from the Ediacaran System in South China: Insights into the Origins of Depositional and Post-Depositional Fluids. *Chem. Geol.* **2015**, *404*, 71–87.

 doi:10.20944/preprints202603.0481.v1

26. Pourret, O.; Davranche, M. Rare Earth Element Sorption onto Hydrous Manganese Oxide: A Modeling Study. *J. Colloid Interface Sci.* **2013**, *395*, 18–23, doi:10.1016/j.jcis.2012.11.054.
27. Wang, D.; Chakraborty, S.; Weindorf, D.C.; Li, B.; Sharma, A.; Paul, S.; Ali, M.N. Synthesized Use of VisNIR DRS and PXRF for Soil Characterization: Total Carbon and Total Nitrogen. *Geoderma* **2015**, *243*, 157–167.
28. Andreetta, A.; Cecchini, G.; Carnicelli, S. Forest Humus Forms in Italy: A Research Approach. *Appl. Soil Ecol.* **2018**, *123*, 384–390, doi:10.1016/j.apsoil.2017.09.029.
29. Ponge, J.-F. Humus Forms in Terrestrial Ecosystems: A Framework to Biodiversity. *Soil Biol. Biochem.* **2003**, *35*, 935–945, doi:10.1016/S0038-0717(03)00149-4.
30. Zhao, X.Q.; Shen, R.F. Aluminum–Nitrogen Interactions in the Soil–Plant System. *Front. Plant Sci.* **2018**, *9*, 807, doi:10.3389/fpls.2018.00807.
31. Montemagno, A.; Bense, V.; Hissler, C.; Ziebel, J. Selective Release and Sequestration of Nutrients and Rare Earth Elements Operated by Litter during the Degradation. In Proceedings of the Goldschmidt2021 abstracts; European Association of Geochemistry: Virtual, 2021.